PNAS

Supplementary Information for

Functional interrogation of lymphocyte subsets in alopecia areata using single-cell RNA sequencing

Eunice Y. Lee,[1,2,6] Zhenpeng Dai,[1,6], Abhinav Jaiswal[3], Eddy Hsi Chun Wang,[1] Niroshana Anandasabapathy[3,4], Angela M. Christiano[1,5,*]

Affiliations:

[1]Department of Dermatology, Columbia University Irving Medical Center. New York, NY, USA.

[2]Medical Scientist Training Program, Columbia University. New York, NY, USA.

[3]Department of Dermatology, Weill Cornell Medicine. New York, NY, USA.

[4]Department of Microbiology and Immunology, Weill Cornell Medicine. New York, NY, USA.

[5]Department of Genetics & Development, Columbia University Irving Medical Center; New York, NY 10032.

[6]These authors contributed equally to this work.

*Corresponding author: Angela M. Christiano. **Email:** amc65@cumc.columbia.edu

This PDF file includes:

Supplementary Materials and Methods
Figures S1 to S8
Tables S1 to S2
SI References

Supplementary Materials and Methods

Preparation of single-cell suspensions from mouse skin After mice were euthanized in accordance with Columbia University IACUC guidelines, hair was shaved using a clipper. The dorsal skin was isolated, subcutaneous fat was removed, and was cut into small pieces prior to digestion with 0.25% collagenase type IV (Sigma-Aldrich, #C5138) in Dulbecco's Modified Eagle Medium (DMEM; Thermo Fisher Scientific, #21068028) at 37°C for 1 hour in a shaking incubator. Collagenase was neutralized with Advanced RPMI 1640 Medium (Fisher Scientific, #12-633-012) + 10% FBS (Gibco, #16000044) and the digested skin was passed through a 70μm strainer. The flow through was rinsed twice with centrifugation at 350*g*, 4°C.

Fluorescence-activated cell sorting (FACS) for scRNAseq For mouse skin single-cell suspensions, cells were resuspended and washed in 2% FBS in Cell Staining Buffer (BioLegend, #420201), then incubated with FITC-anti-mouse CD45 antibody (BioLegend, #103108) at a 1:100 dilution for 30 minutes on ice. Cells were washed in 2% FBS/Cell Staining Buffer and strained through a 50-μm filter. Prior to FACS, cells were stained with propidium iodide (Fisher Scientific, #00-6990-50; 1:500). Live CD45+ cells (FITC+, propidium iodide-) were isolated for subsequent scRNAseq. For human skin single-cell suspensions, cells were resuspended and washed in 2% FBS in Cell Staining Buffer, then stained with DRAQ5 (BioLegend, #424201; 1:1000) and SYTOX-Green (Thermo Fisher Scientific, #S7020; 1:500) prior to FACS isolation for DRAQ5- SYTOX-Green- live cells.

Flow cytometry Single-cell suspensions were resuspended and washed in 2% FBS in Cell Staining Buffer, then stained with LIVE/DEAD Fixable Blue Dead Cell Stain Kit (Thermo Fisher Scientific, #L34962) according to the manufacturer's protocol. For surface marker staining, cells were incubated with antibodies at 1:200 in the dark on ice for 30 minutes. For intracellular staining, cells were fixed, permeabilized, and stained using the FOXP3/Transcription Factor Staining Buffer Set Kit (Thermo Fisher Scientific, #00-5523-00) and its accompanying protocol. Antibodies for intracellular staining were diluted at 1:200. A list of antibodies can be found in Table S3.

T_{reg} suppression assay $CD25^{hi}$ CD4+ T_{reg} and non-T_{reg} T cells were isolated from the skin-draining lymph nodes of grafted C3H/HeJ mice with AA and UG controls on an Influx cell sorter. Non-T_{reg} T cells were labeled with 2.5 μM CellTrace Violet, cultured with the T_{regs} at various ratios, and stimulated with plated-bound anti-CD3 (1 μg/ml) (Bio X Cell; 145-2C11) and anti-CD28 (2 μg/ml) (Bio X Cell; 37.51) in a flat-bottom 96-well plate (Thermo Fisher Scientific) for 4 days. Percent suppression of effector T cell proliferation was calculated according to previous reports (1).

Processing and analysis of scRNAseq data FASTQ files were aligned using the CellRanger pipeline (v3.0.1 and mm10 reference genome for mouse scRNAseq experiments, v3.0.2 and GRCh38 reference genome for human scRNAseq experiments). CellRanger outputs (barcodes.tsv, genes.tsv, and matrix.mts) for each sample were loaded into R (version 4.1.1), where cells were subject to further quality control methods using the Seurat package (version 4.0.4) (2, 3). For the mouse dataset, we filtered cells to exclude low quality cells and doublets with > 15% mitochondrial RNA content, < 200 unique molecular identifier (UMI) counts, and/or > 5000 UMI counts. For the human dataset, we excluded cells with > 10% mitochondrial RNA content, < 200 UMI counts, and/or > 4000 UMI counts. The distribution of mitochondrial RNA content, UMI counts, and unique gene counts across samples after quality control filtering is shown in SI Appendix, Fig. S1B.

The Seurat package was then used to merge samples into a single dataset and perform downstream analyses. Gene expression matrices were processed via the 'SCTransform' function for normalization, identification of highly variable genes, and to regress out unwanted sources of variation (i.e. UMI counts and mitochondrial RNA content) (4). Batch effects were corrected using the canonical correlation analysis (CCA) workflow (2, 3). Then, using the top 3000 highly variable genes identified via SCTransform, we performed a principal component analysis (PCA). The first 30 principal components were used to perform uniform manifold approximation and projection (UMAP) dimensionality reduction into a 2-dimensional visualization space.

Following UMAP reduction, unsupervised clustering was performed as described in Obradovic et al. (2021) (5). Briefly, we used the 'FindClusters' function to cluster the dataset with resolution values from 0.01 to 1.0 at intervals of 0.01. At each resolution, we computed a silhouette score based on a subsampling of 1000 clustered cells, and used this value to select an optimum resolution within this range. This method

was utilized to control for over-clustering, since the FindClusters function allows for arbitrary selection of resolution values for clustering. We annotated clusters based on the expression of canonical markers (i.e. *Cd8a or Cd8b1* expression for CD8 T cells), the top enriched genes relative to other clusters (identified using the Seurat 'FindAllMarkers' function), and the SingleR R package (version 1.6.1) (6). For the SingleR analysis, we specifically used the mouse bulk RNA sequencing dataset from the Immunological Genome Project for the mouse dataset and the Human Primary Cell Atlas for the human dataset (7, 8). Differential gene expression (DGE) analyses were performed using the Seurat 'FindMarkers' command and the Model-based Analysis of Single Cell Transcriptomics (MAST) method (9). When applicable, gene set enrichment analysis (GSEA) using DGE outputs was performed using the clusterProfiler R package (version 4.0.5).

To assess changes in the distribution of T lymphocytes and T lymphocyte subsets between AA and UG/CTRL, we first identified each population based on canonical markers established in the literature. For instance, murine T cells were defined as cells expressing *Cd3e/Cd3d/Cd3g*. CD8+ T cells were defined based on co-expression of *Cd3e/Cd3d/Cd3g* and *Cd8a/Cd8b1*, with no expression of *Cd4*. CD4+ T_h cells co- expressed *Cd3e/Cd3d/Cd3g* and *Cd4*, with no expression of *Cd8a/Cd8b1* and *Foxp3*. CD4+ T_{reg} co-expressed *Cd3e/Cd3d/Cd3g*, *Cd4*, and *Foxp3* with no expression of *Cd8a/Cd8b1* and *Foxp3*. NK T cells were defined as cells in Cluster 6, which represented NK/NKT cells, that expressed *Cd3e/Cd3d/Cd3g*. γδ T cells were defined as cells that co-expressed *Cd3e/Cd3d/Cd3g* with genes encoding components of the γδ TCR chain, such as *Trdc* and *Trdv1*. Human T cells and T cell subsets were identified using the human homologs of the mouse genes.

To perform pseudotime trajectory analysis, we employed the monocle R package (version 2.20.0) (10, 11). Cells were ordered using the top highly variable genes identified via the 'SCTransform' function in Seurat, as described above. Kinetic scoring analyses for CD8+ T cell subsets were performed as described in Jaiswal et al. (2022) (12). Briefly, expression matrices from datasets of LCMV infection (GEO: GSE10239, GEO: GSE41867), vaccinia virus infection (GEO: GSE79805), and human yellow fever vaccination (GEO: GSE26347, GEO: GSE100745) were transformed into a log2 (normalized intensity + 1) format for microarrays and a log2(FPKM + 1) for RNA sequencing datasets (13–16). Transformed matrices were then filtered on genes with at least one read mapped across all samples. For each timepoint, the signature enrichment was compared to the immediately preceding timepoint. For the LCMV infection and the GEO:

GSE26347 yellow fever dataset, significance was calculated via mixed-effects modeling using the lme function from the nmle package in R, with a random a random intercept considered for each sample scored. For the vaccinia virus infection, the slope of gene enrichment (shaded) was calculated using lm. *$p < 0.05$; **$p < 0.01$; ***$p < 0.001$; ****$p < 0.0001$. For the GEO: GSE100745 yellow fever dataset, significance values for enrichment at a given time point versus the time point preceding it were calculated using a Student's t-test.

Supplementary Figures

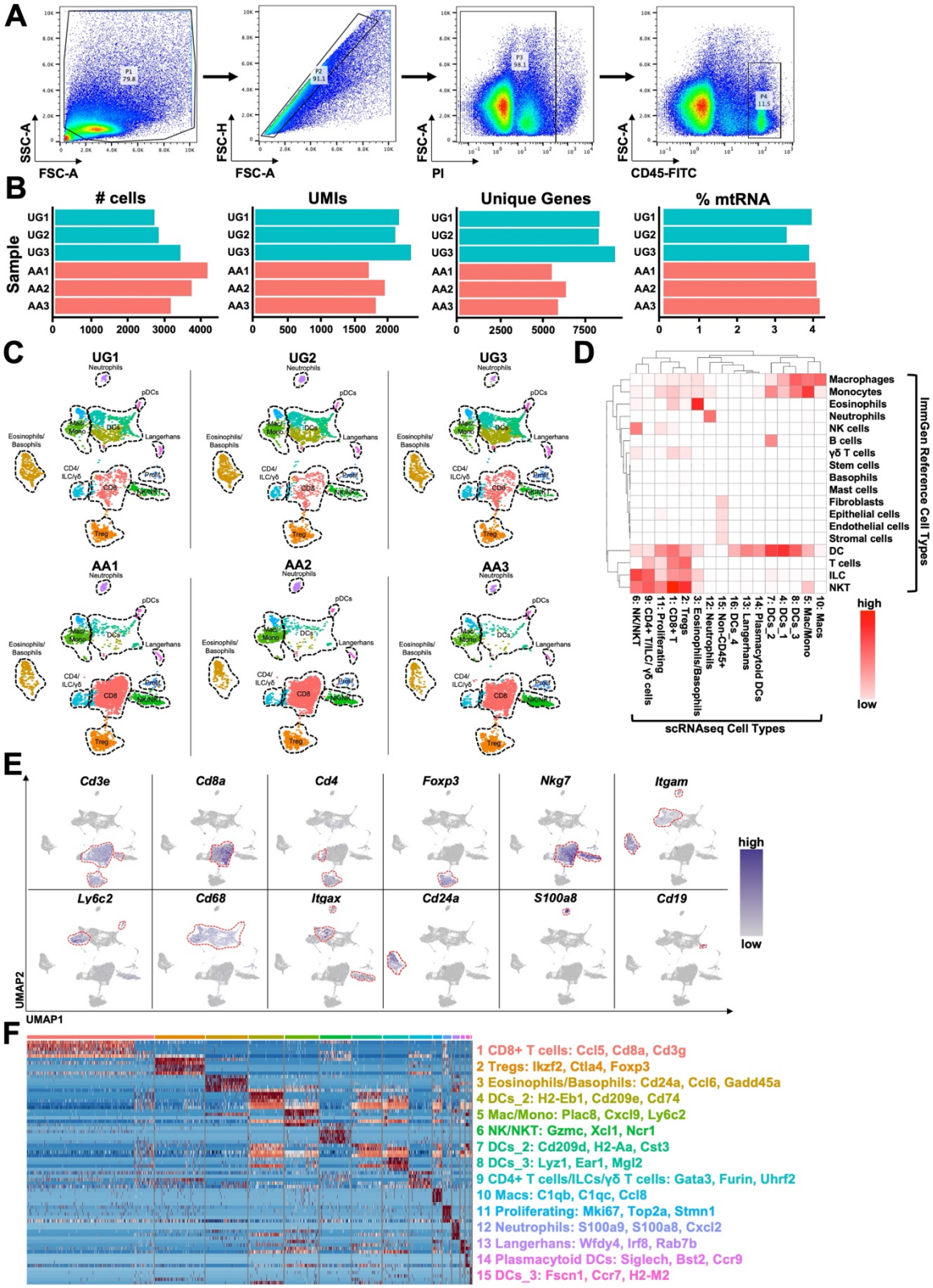

Fig. S1. Quality control and annotation of scRNAseq data from CD45+ skin immune cells in murine AA. A) Representative plots showing FACS isolation of live CD45+ cells for scRNAseq. B) Number of cells, UMIs, genes, and mitochondrial RNA content in scRNAseq data across the six sequenced samples. C) Heatmap of normalized correction values for predicted cell types based on the SingleR R package, using the mouse Immunological Genome Project microarray dataset as a reference (6, 7). D) UMAPs for each individual sample in the combined scRNAseq E) Expression of canonical marker genes for each cell type (i.e. *Cd3e* is a marker of T cells; *Cd8a* is a marker of CD8+ T cells). F) Heatmap of top highly expressed genes in each cluster. dataset. Data from each sample was aligned using the canonical correlational analysis function in the Seurat R package.

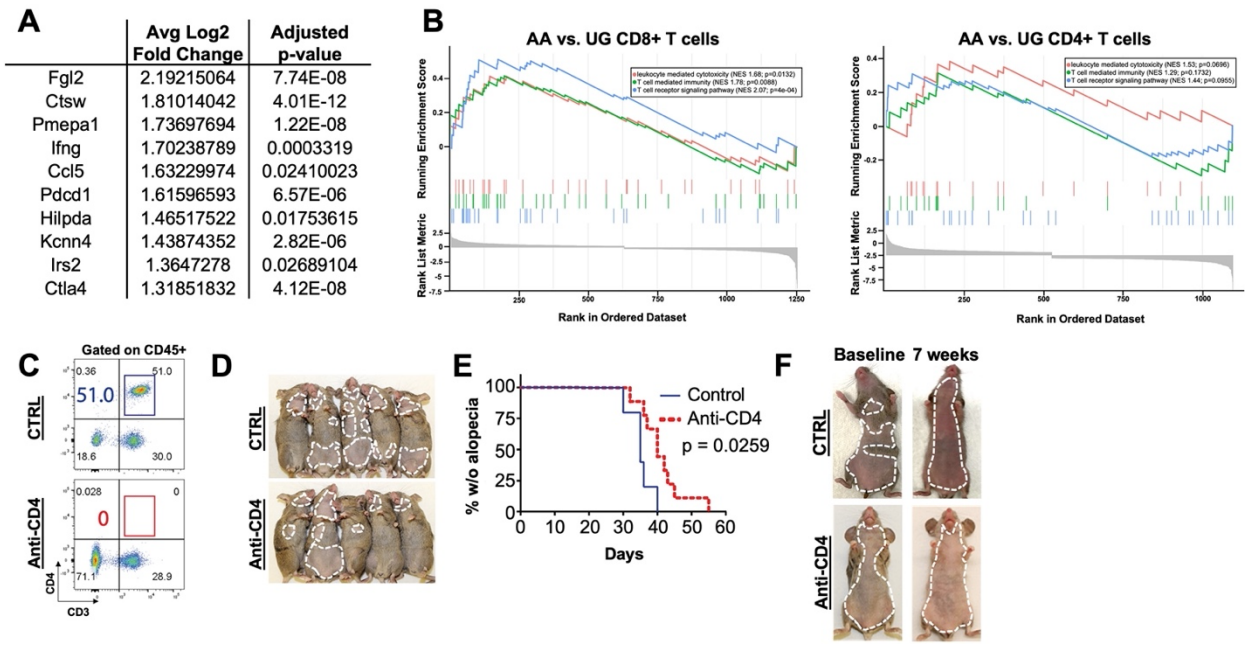

Fig. S2. Depletion of CD4+ T cells delays AA, but does not prevent or reverse disease. A) Top 10 genes upregulated in AA-associated CD4+ T cells compared to UG-associated CD4+ T cells in differential gene expression analysis. Both genes associated with T cell activation (*Ctsw*, *Ifng*, *Ccl5*) and those associated with T_{reg} function (*Fgl2*, *Pdcd1*, *Ctla4*) were upregulated in AA CD4+ T cells. B) GSEA for gene signatures associated with leukocyte mediated cytotoxicity, T cell mediated immunity, and T cell receptor signaling using differentially expressed genes between CD8+ and CD4+ T cells across disease conditions. Note higher Note AA-associated CD8+ T cells show higher Normalized Enrichment Scores (NES) with $p < 0.05$, whereas CD4+ T cells show lower NES with $p > 0.05$. C) Treatment of grafted C3H/HeJ mice with anti-CD4 efficiently depleted CD4+ T cells compared to isotype control. D) Anti-CD4 administration in grafted C3H/HeJ mice prior to hair loss onset delayed disease development relative to isotype control. E) Kaplan-Meier curve for experiment shown in D). F) Anti-CD4 administration in grafted C3H/HeJ mice with established disease had no effect on disease progression. Both anti-CD4 and isotype control groups progressed to total body hair loss by 7 weeks from the onset of treatment.

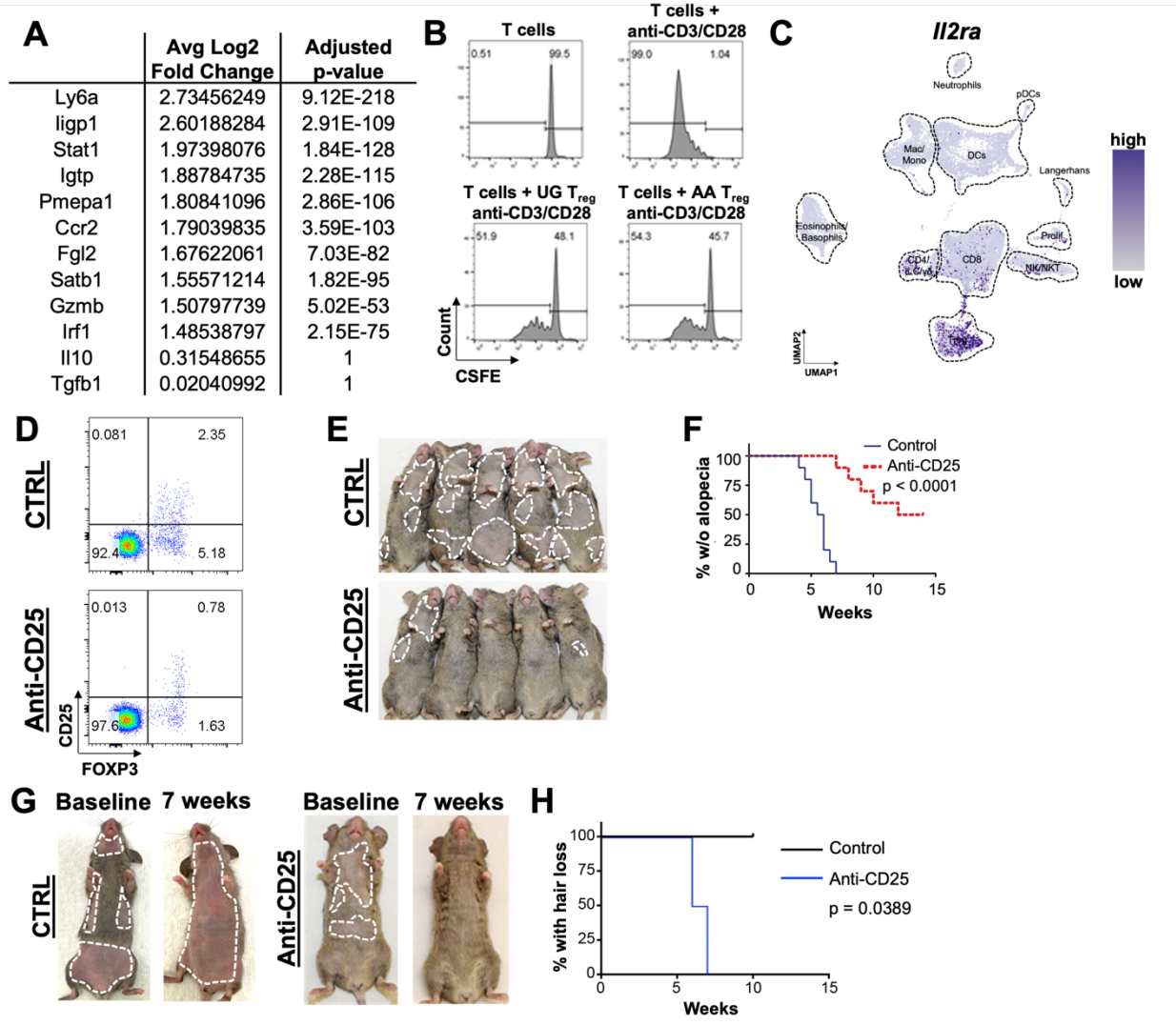

	Avg Log2 Fold Change	Adjusted p-value
Ly6a	2.73456249	9.12E-218
Iigp1	2.60188284	2.91E-109
Stat1	1.97398076	1.84E-128
Igtp	1.88784735	2.28E-115
Pmepa1	1.80841096	2.86E-106
Ccr2	1.79039835	3.59E-103
Fgl2	1.67622061	7.03E-82
Satb1	1.55571214	1.82E-95
Gzmb	1.50797739	5.02E-53
Irf1	1.48538797	2.15E-75
Il10	0.31548655	1
Tgfb1	0.02040992	1

Fig. S3. CD25+ T cells are required for AA onset and progression. A) Differential gene expression analysis between AA and UG T_{reg}, showing the top 10 genes upregulated in AA T_{reg} as well as *Il10* and *Tgfb1*, which encode anti-inflammatory cytokines important for T_{reg}-mediated immunosuppression. Note there is no statistically significant difference in the expression of *Il10* and *Tfgb1.* B) CellTrace Violet (CSFE)-labeled T cells isolated from the skin-draining lymph nodes (SDLN) of UG mice were cultured alone, alone with anti-CD3/CD28 stimulation, or in the presence of UG T_{reg} or AA T_{reg} alongside anti-CD3/CD28 stimulation. T_{reg} suppressive capacity was assessed by flow cytometry of CFSE levels in labeled T cells. C) Expression of *Il2ra* (CD25) in scRNAseq data of CD45+ skin immune cells in murine AA. D) Anti-CD25 administration depleted CD25+ cells in treated mice relative to mice treated with isotype control. E) Anti-CD25 administration in grafted C3H/HeJ mice prior to AA onset prevented disease. F) Kaplan-Meier curve

for experiment shown in E). G) Anti-CD25 administration in grafted C3H/HeJ mice with established AA reversed disease compared to those treated with isotype control. H) Kaplan-Meier curve for experiment shown in G).

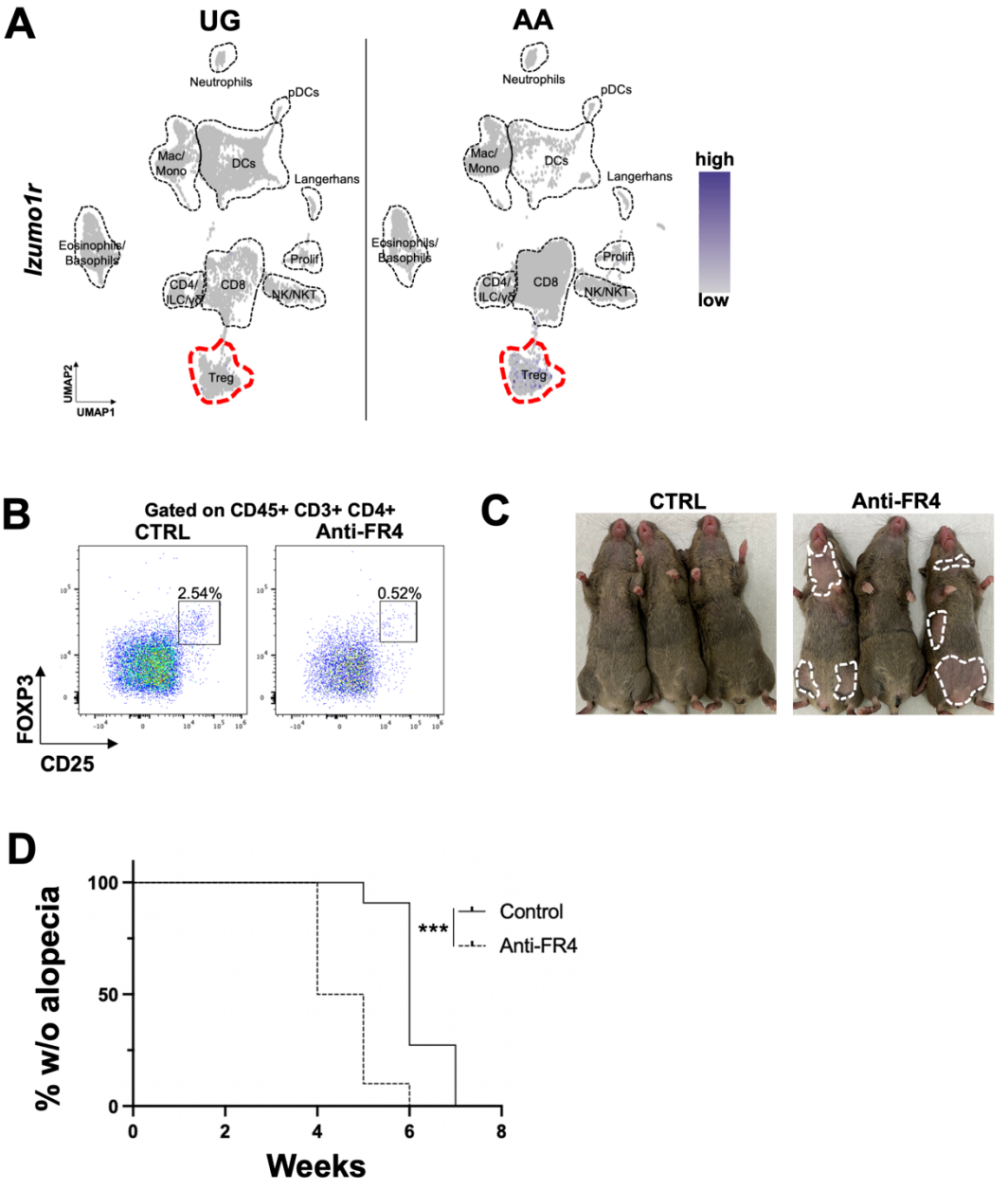

Fig. S4. FR4+ T_{reg} are protective in AA. A) Expression of *Izumo1r* overlaid onto the overall CD45+ UMAP for each disease condition, showing specific localization of *Izumo1r* expression in the CD4+ T_{reg} cluster. B) Anti-FR4 administration depleted FoxP3+ CD25+ T_{reg} relative to mice treated with isotype control. Gated on CD45+ CD3+ CD4+. C) Anti-FR4 administration in grafted C3H/HeJ mice prior to the occurrence of hair loss accelerated disease onset relative to isotype control. D) Kaplan-Meier curve for experiment shown in C). *p < 0.05; **p < 0.01; ***p < 0.001; ****p < 0.0001.

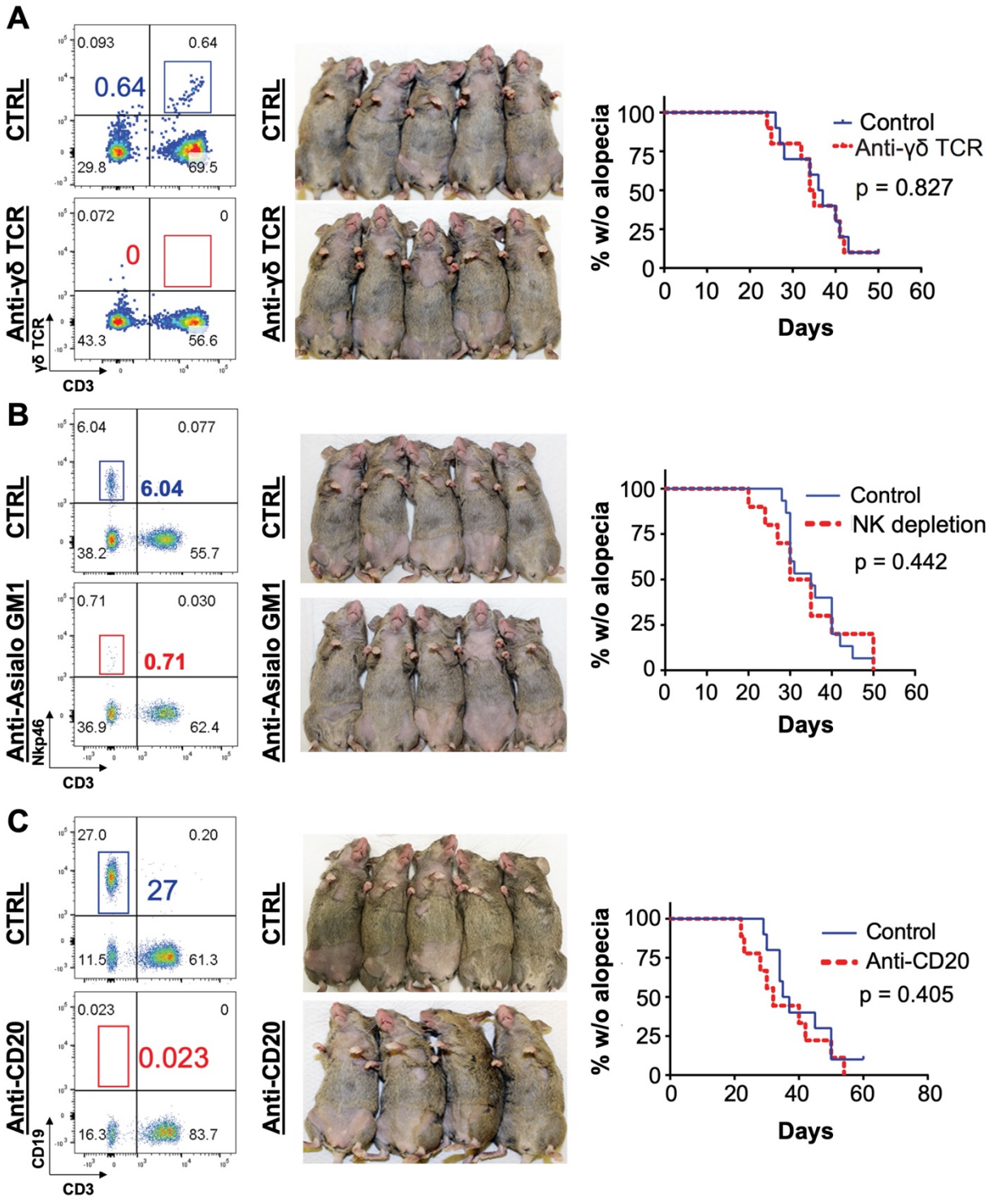

Figure S5. Depletion of γδ T cells, NK cells, and B cells has no effect on AA development. A) Anti-γδ TCR depletion in grafted C3H/HeJ mice prior to the development of AA. B) Anti-Asialo GM1 depletion in

grafted C3H/HeJ mice prior to the development of AA to target NK cells. C) Anti-CD20 depletion in grafted C3H/HeJ mice prior to the development of AA to target B cells. Left, flow cytometry showing efficient depletion upon treatment with antibody of interest, relative to isotype control; Middle, depletion had no effect on disease onset; Right, Kaplan-Meier curve for depletion experiment.

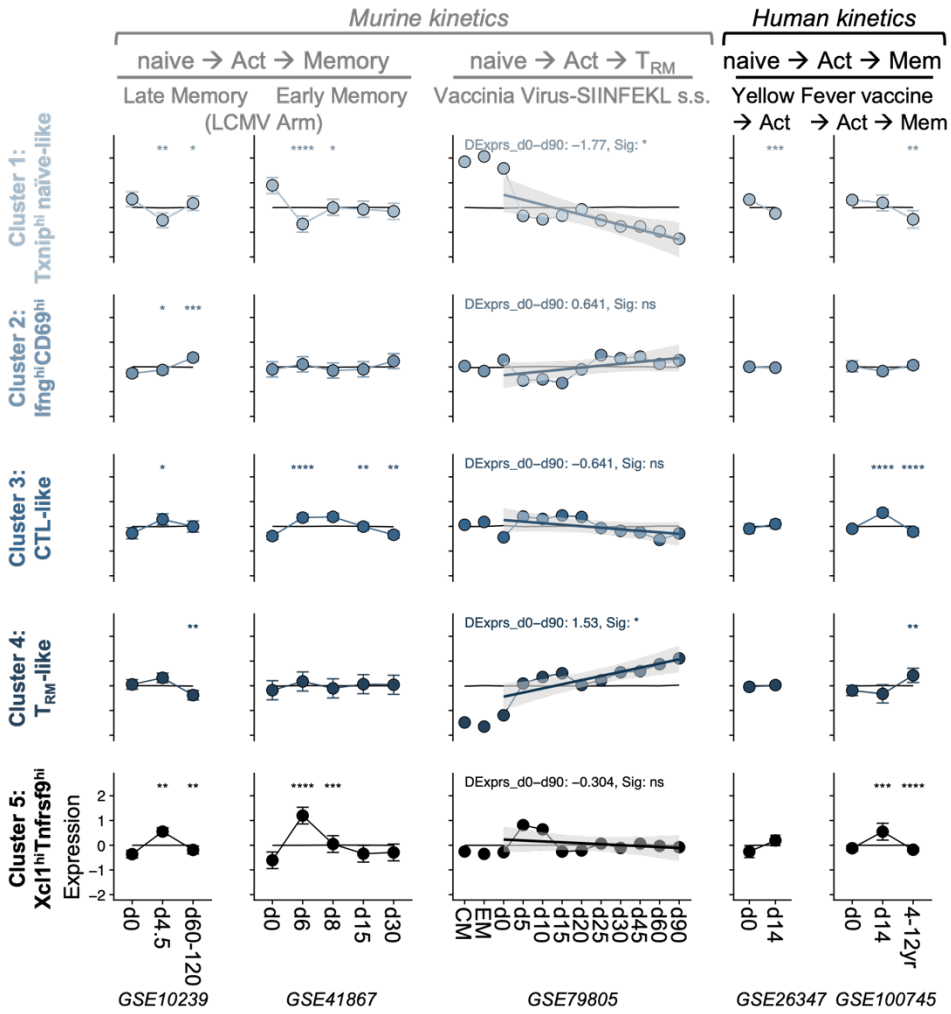

Figure S6. Scoring transcriptome of AA murine CD8+ T cells into canonical T cell differentiation trajectories. The transcriptional signature of each of the five CD8+ T cells in murine AA skin was scored against CD8+ T cell signatures derived from murine LCMV infection, murine vaccinia virus infection, and human YF vaccination at various time points that span T cell differentiation from naïve, activation, and memory states. Significance values are shown for the comparison between enrichment at a given time point and the immediately preceding time point. For the vaccinia virus infection, the slope of gene enrichment (shaded) was calculated using lm, with slopes and significance values annotated. *p < 0.05; **p < 0.01; ***p < 0.001; ****p < 0.0001.

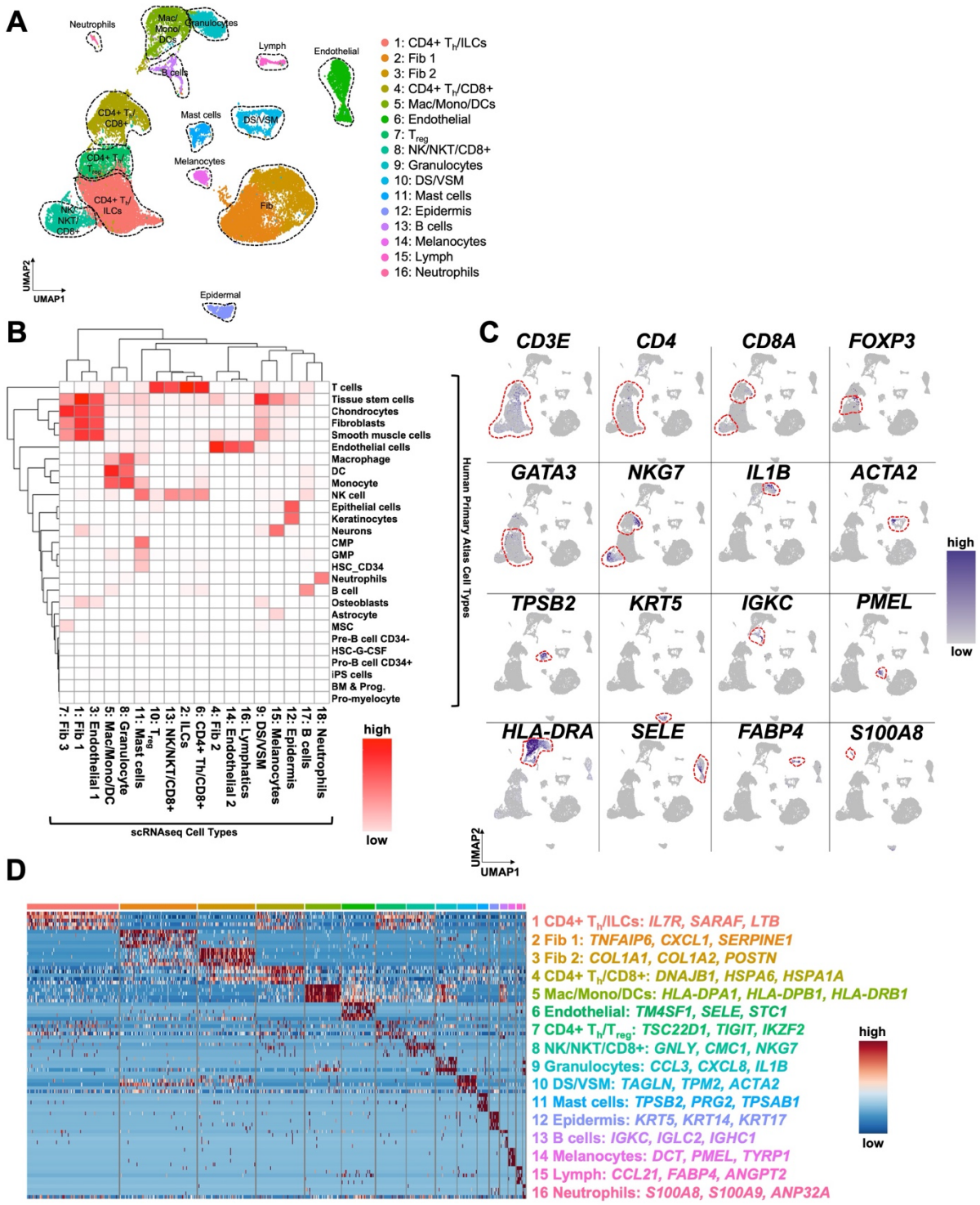

Figure S7. scRNAseq of human AA. A) UMAP of scRNAseq data obtained from scalp biopsies of 5 AA patients and 2 healthy controls. Unsupervised clustering of 32,134 cells (21,766 AA; 32,134 CTRL) after quality control and CCA- based alignment uncovered 16 distinct populations. B) Heatmap of normalized

correction values for SingleR-based predictions for the identity of each cluster, using the Human Primary Cell Atlas microarray dataset as a reference (6, 8). C) Expression of canonical marker genes for each cell type (i.e. *CD3E* is a marker of T cells; *CD8A* is a marker of CD8+ T cells). D) Heatmap of top highly expressed genes in each cluster. CMP, common myeloid progenitors; DC, dendritic cells; DS, dermal sheath; Fib, fibroblasts; GMP, granulocyte myeloid progenitors; G-CSF, granulocyte colony-stimulating factor; HSC, hematopoietic stem cells; ILC, innate lymphoid cells; iPS, induced pluripotent stem cells; Lymph, lymphatic vessel; Mac, macrophages; Mono, monocytes; NK, natural killer cells; NKT, natural killer T cells; T_h, helper T cells; T_{reg}, regulatory T cells; VSM, vascular smooth muscle.

A Upregulated in AA CD8+ T cells (relative to CTRL CD8+ T cells)

	Avg Log2 Fold Change	Adjusted p-value
GIMAP4	1.39846555	3.71E-10
TIGIT	1.27554788	3.20E-08
KLRK1	1.10187751	2.18E-09
CLEC2D	0.96822988	0.00019814
LINC00623	0.96465985	8.88E-06
GZMK	0.96125549	0.00215799
LYAR	0.92156419	0.00256258
IL32	0.89261535	0.00270047
PIK3R1	0.87295165	0.00037971
SUB1	0.86996308	6.43E-09

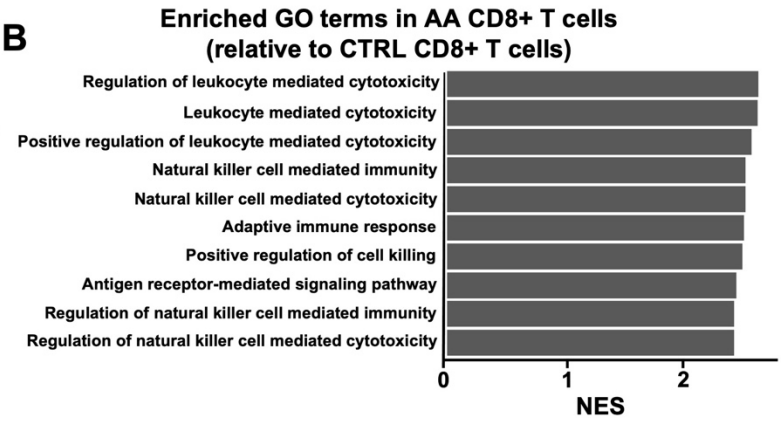

C Upregulated in AA CD4+ T_h (relative to CTRL CD4+ T_h)

	Avg Log2 Fold Change	Adjusted p-value
IL32	1.73969853	3.07E-08
RPS26	1.6448595	7.72E-26
TSC22D3	1.49531907	2.79E-10
IL7R	1.40525224	1.07E-10
CXCR4	1.33473934	1.04E-12
CD2	1.25486994	7.96E-15
BCL11B	1.17238645	2.37E-12
FYB1	1.15068149	2.86E-08
CD69	1.1439799	9.20E-05
LTB	1.12994206	3.81E-14

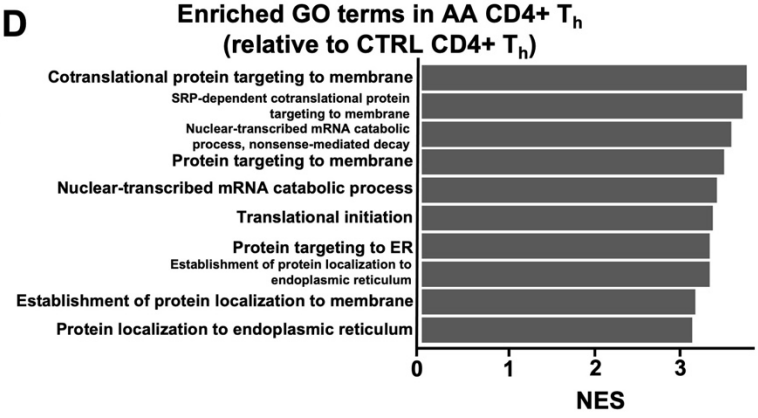

Figure S8. Differentially expressed genes in CD4+ T_h and CD8+ T cells between AA and CTRL. A) Top upregulated genes in AA CD8+ T cells relative to CTRL CD8+ T cells. B) Top statistically significant enriched GO terms in AA CD8+ T cells as identified by GSEA of differentially expressed genes between AA and CTRL CD8+ T cells, arranged via descending NES. C) Top upregulated genes in AA CD4+ Th relative to CTRL CD4+ T_h. D) Top statistically significant enriched GO terms in AA CD4+ T_h as identified by GSEA of differentially expressed genes between AA and CTRL CD4+ T_h, arranged via descending NES.

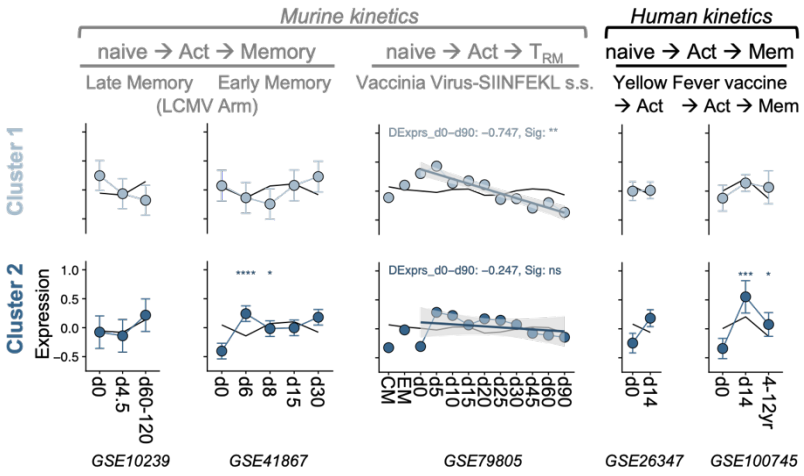

Figure S9. Scoring transcriptome of AA human CD8+ T cells into canonical T cell differentiation trajectories. The transcriptional signature of the two CD8+ T cell subsets in human AA skin was scored against CD8+ T cell signatures derived from murine LCMV infection, murine vaccinia virus infection, and human YF vaccination at various time points that span T cell differentiation from naïve, activation, and memory states. Significance values are shown for the comparison between enrichment at a given time point and the immediately preceding time point. *p < 0.05; **p < 0.01; ***p < 0.001; ****p < 0.0001.

Table S1. Signature genes for murine CD8+ T cell subsets.

Circulating (17, 18)	CD8_NaiveLike (19)	CD8_EarlyActive (19)	Effector (17, 18)	Trm (17, 18)
1700025G04Rik	Ccr7	Gzmk	1700017B05Rik	2900026A02Rik
3110052M02Rik	Il7r	Fos	Cd86	AA467197
2010012O05Rik	Sell	Cd69	Ezh2	Abcb1b
A430078G23Rik	Tcf7	Zfp36	Itgb1	Adam19
Acss1	Txk	Fosb	Prr13	Atf3
Aff3	S1pr1	Ccl5	Top2a	B4galnt4
Apobec2	Lef1	Gzmm	2010002N04Rik	Bag3
Arhgap26	Satb1	Dusp2	Cdc20b	Bhlhe40
Arhgef18		Lyar	F630043A04Rik	Btg2
Armc7		Samd3	Jup	Btg3
As3mt		Cxcr4	Prr5l	Ccl4
Aven		Ctsw	Tpx2	Cd244
B3gnt5		Cd8a	2010012O05Rik	Cd69
Bin2		Anxa1	Cdc25b	Cdh1
Car5b		Klrg1	Fam129a	Chd7
Cdc14b		Cd8b1	Kif11	Chn2
Cmah		Aoah	Prune	Cish
D1Ertd622		Tagap	Trdn	Coq10b
Dapl1		Klrd1	2610029I01Rik	Cpd
Dennd2d		Ier2	Cdk1	Crem
Dgka		Gzma	Fancm	Ctla4
Dnahc8		Cst7	Kif15	Dennd4a
Dock5		Itm2c	Ptms	Dgat1
Dusp7		Parp8	Trio	Dnaja1
Ehd3		Btg2	2810417H13Rik	Dnaja4
Elovl7			Cdk2	Dnajb1
Eomes			Fhl2	Dnajb4
F2rl2			Kif22	Dnajb6
Fam49a			Pus10	Dusp1
Fam53b			Tspan2	Dusp4
Fam65b			2810417H13Rik	Dusp6
Fgf13			Cenpa	Egr1
Flna			Fkbp5	Ehd1
Gab3			Kif23	Ell2
Gm11435			Pycard	Fasl
Gramd4			Tspan32	Fbxo30
Gzmm			3110052M02Rik	Fgl2

Haao			Cenpe	Fmnl3
Icam2			Gabarapl1	Fos
Il17ra			Klra10	Fosl2
Il18rap			Rab11fip4	Gabarapl1
Kbtbd11			Ubash3b	Gadd45b
Kcnj8			4930447A16Rik	Gem
Klf2			Cenpk	Glrx
Klhdc1			Galnt3	Gpr171
Klrb1c			Klra3	Gpr56
Klrg1			Racgap1	Gzmb
Lair1			Unc119	H3f3b
Lfng			4930515G01Rik	Havcr2
Limd1			Cep55	Hip1
Lpin1			Gem	Hpgds
Ly9			Klra6	Hsp90aa1
Mboat1			Rap1gap2	Hspa5
Ms4a4c			Usp3	Icos
Nck2			4930547N16Rik	Ifng
Nfatc3			Cep76	Ifrd1
Nod1			Glcci1	Il21r
Nsg2			Klra8	Il4ra
Pde2a			Rbms1	Inpp4b
Pion			Usp46	Irf4
Prss12			6330403K07Rik	Isg20
Prune			Cercam	Isy1
Pycard			Gm10286	Igta1
Qprt			Klre1	Jun
Rap1gap2			Reep5	Junb
Rasa3			Whsc1	Kdm6b
Rasgrp2			A630007B06Rik	Litaf
Rgs19			Chd7	Lmnb1
S1pr1			Gm10785	Ly6g5b
S1pr4			Klrg1	Mxd1
Samd3			Rhoq	Mxi1
Sell			Xlr	Neurl3
Sfxn3			Adam17	Nfil3
Sh2d1a			Chn2	Nfkbie
Sh3bp5			Gm10786	Nr4a1
Sidt1			Kntc1	Nr4a2

Sike1			Rnf19a	Nr4a3
Slamf6			Xpnpep1	Ntan1
Smpdl3b			Ahnak	Odc1
Spn			Chsy1	P2ry10
Stard10			Gm11277	P4hb
Tcf7			Lag3	Pdcd1
Tlr1			Rnf216	Per1
Tmem71			Zeb2	Plk3
Tnfrsf26			AI597468	Plscr1
Traf3ip3			Cited2	Pmepa1
Ubxn2b			Gm14005	Pp1r15a
Usp33			Lamc1	Prdx6
Ypel1			Rnpep	Ptp4a1
Zeb2			Zfand5	Qpct
Zfp595			Ak3	Rbpj
Zfp760			Cldnd2	Rgs1
			Gm4884	Rgs10
			Lass6	Rgs16
			Rora	Rhob
			Zfp40	Rnf149
			Alcam	Rrad
			Cmklr1	Sik1
			Gm8615	Skil
			Lgals1	Slc16a6
			Rrm2	Slc7a5
			Zfp874b	Spty2d1
			Anln	Ssbp2
			Cmpk1	Stk17b
			Gna15	Tgif1
			Lgals3	Tigit
			S100a4	Tiparp
			Anxa4	Tjp1
			Cry1	Tnf
			Gpx8	Tnfaip3
			Lmnb1	Tnfrsf1b
			S1pr5	Tnfrsf9
			Apaf1	Tra2a
			Crybg3	Trib1
			Grxcr1	Trp53inp2

			LOC100503984	Ube2s
			Scd2	Vps37b
			Apobec2	Wsb1
			Csda	Xcl1
			Gsn	Zfand5
			Lxn	Zfp36l1
			Serinc5	
			Arhgap11a	
			Csnk1e	
			Gzma	
			Manba	
			Serpinb6b	
			Arhgap19	
			Ctnnbip1	
			Gzmb	
			Mki67	
			Shcbp1	
			Arhgef12	
			Ctsc	
			Gzmk	
			Msc	
			Slc25a20	
			Arntl	
			Cx3cr1	
			Havcr2	
			Mxi1	
			Slc25a33	
			Art2a-ps	
			Cyp3a16	
			Hbb-b2	
			Ncapg	
			Slc25a45	
			As3mt	
			D330041H03Rik	
			Hiatl1	
			Ndnl2	
			Slc4a7	
			Asna1	
			Dapk2	

			Hist1h1b	
			Nebl	
			Snx10	
			Atoh1	
			Dclk2	
			Hist1h2ab	
			Nipal3	
			Snx5	
			Atp2a3	
			Ddx19b	
			Hist1h2ak	
			Nqo2	
			Sord	
			Atp6v1d	
			Ddx28	
			Hist1h2bf	
			Nrp1	
			Sp140	
			AU022870	
			Dennd5a	
			Hist1h2bj	
			Olfr598	
			Spag1	
			BC013712	
			Depdc1a	
			Hist1h2bk	
			Olfr766	
			Spag5	
			Bhlhe40	
			Depdc1b	
			Hist1h2bm	
			Osbpl3	
			Spast	
			Bub1	
			Dhx40	
			Hist1h2bn	
			Osbpl8	
			Spc25	
			Bub1b	

			Dlgap5	
			Hmgb2	
			Palm	
			Spn	
			C330027C09Rik	
			Dnajc1	
			I830127L07Rik	
			Pdcd1	
			Sptlc2	
			Car5b	
			Dock5	
			Icos	
			Pgm2l1	
			Stmn1	
			Carhsp1	
			Dtl	
			Idh2	
			Pld4	
			Stx11	
			Casc5	
			Dync1li2	
			Igf2bp3	
			Plek	
			Sun1	
			Casp3	
			E2f2	
			Il18rap	
			Plekhf1	
			Suox	
			Casp7	
			E2f8	
			Inpp4a	
			Plekho1	
			Swap70	
			Ccna2	
			Efhd2	
			Irf4	
			Pmaip1	
			Tbcc	

			Ccnb1	
			Emp1	
			Itga2	
			Pola1	
			Tbkbp1	
			Ccnb2	
			Ern1	
			Itga4	
			Prc1	
			Timp2	
			Ccne2	
			Esm1	
			Itgam	
			Prdm1	
			Tmem165	
			Cd68	
			Etfb	
			Itgax	
			Prdx4	
			Tmf1	

Table S2. List of antibodies used in the study.

Name	Clone	Company	Catalog No.	Use
anti-mouse CD45-A700	30-F11	BD	BDB560510	Flow Cytometry
anti-mouse CD45-FITC	30-F11	BioLegend	103108	Flow Cytometry
anti-mouse CD3-BV421	17A2	BioLegend	100227	Flow Cytometry
anti-mouse CD3-PerCP	17A2	Fisher Scientific	46-0032-82	Flow Cytometry
anti-mouse CD3-PE-Dazzle 594	17A2	BioLegend	100245	Flow Cytometry
anti-mouse CD3-PE/Cy7	17A2	BioLegend	100219	Flow Cytometry
anti-mouse CD4-PerCP	GK1.5	BioLegend	100431	Flow Cytometry
anti-mouse CD4-BV711	GK1.5	BioLegend	100447	Flow Cytometry
anti-mouse CD8α-BV605	53-6.7	BioLegend	100743	Flow Cytometry
anti-mouse CD8β-APC	53-5.8	BioLegend	140410	Flow Cytometry
anti-mouse CD19-APC	1D3	BioLegend	152409	Flow Cytometry
anti-mouse Nkp46-BV421	29A1.4	BioLegend	137611	Flow Cytometry
anti-mouse CD25-APC-eFluor 780	PC61.5	eBioscience	47-0251-82	Flow Cytometry
anti-mouse CD25-BV421	PC61	BD	562606	Flow Cytometry
anti-mouse FoxP3-FITC	FJK-16s	Thermo Fisher Scientific	11-5773-82	Flow Cytometry
anti-mouse FoxP3-PE-eFluor 610	FJK-16s	Thermo Fisher Scientific	61-5773-82	Flow Cytometry
anti-mouse TCRγ-APC	GL3	BioLegend	118116	Flow Cytometry
anti-mouse CD4	GK1.5	Bio X Cell	BE00031	In Vivo Depletion
anti-mouse CD8α	YTS 169.4	Bio X Cell	BP0117	In Vivo Depletion
anti-mouse CD25	PC61	Bio X Cell	BP0012	In Vivo Depletion
anti-mouse CD20	AISB12	Bio X Cell	BE0302	In Vivo Depletion
anti-mouse Asialo GM1	N/A	Fisher Scientific	NC1345696	In Vivo Depletion
anti-mouse FR4	TH6	BioLegend	125111	In Vivo Depletion
ant-mouse TCRγ/δ	UD7-13D5	BioLegend	107502	In Vivo Depletion

SI References

1. A. N. McMurchy, M. K. Levings, Suppression assays with human T regulatory cells: a technical guide. *Eur J Immunol* **42**, 27–34 (2012).

2. A. Butler, P. Hoffman, P. Smibert, E. Papalexi, R. Satija, Integrating single-cell transcriptomic data across different conditions, technologies, and species. *Nat Biotechnol* **36**, 411–420 (2018).

3. T. Stuart, *et al.*, Comprehensive Integration of Single-Cell Data. *Cell* **177**, 1888-1902.e21 (2019).

4. C. Hafemeister, R. Satija, Normalization and variance stabilization of single-cell RNA-seq data using regularized negative binomial regression. *Genome Biology* **20**, 296 (2019).

5. A. Obradovic, *et al.*, Single-cell protein activity analysis identifies recurrence-associated renal tumor macrophages. *Cell* **184**, 2988-3005.e16 (2021).

6. D. Aran, *et al.*, Reference-based analysis of lung single-cell sequencing reveals a transitional profibrotic macrophage. *Nat Immunol* **20**, 163–172 (2019).

7. T. S. P. Heng, M. W. Painter, Immunological Genome Project Consortium, The Immunological Genome Project: networks of gene expression in immune cells. *Nat Immunol* **9**, 1091–1094 (2008).

8. N. A. Mabbott, J. K. Baillie, H. Brown, T. C. Freeman, D. A. Hume, An expression atlas of human primary cells: inference of gene function from coexpression networks. *BMC Genomics* **14**, 632 (2013).

9. G. Finak, *et al.*, MAST: a flexible statistical framework for assessing transcriptional changes and characterizing heterogeneity in single-cell RNA sequencing data. *Genome Biol* **16**, 278 (2015).

10. X. Qiu, *et al.*, Single-cell mRNA quantification and differential analysis with Census. *Nat Methods* **14**, 309–315 (2017).

11. X. Qiu, *et al.*, Reversed graph embedding resolves complex single-cell trajectories. *Nat Methods* **14**, 979–982 (2017).

12. A. Jaiswal, *et al.*, An activation to memory differentiation trajectory of tumor-infiltrating lymphocytes informs metastatic melanoma outcomes. *Cancer Cell* **40**, 524-544.e5 (2022).

13. S. Sarkar, *et al.*, Functional and genomic profiling of effector CD8 T cell subsets with distinct memory fates. *Journal of Experimental Medicine* **205**, 625–640 (2008).

14. T. A. Doering, *et al.*, Network Analysis Reveals Centrally Connected Genes and Pathways Involved in CD8+ T Cell Exhaustion versus Memory. *Immunity* **37**, 1130–1144 (2012).

15. R. S. Akondy, *et al.*, Origin and differentiation of human memory CD8 T cells after vaccination. *Nature* **552**, 362–367 (2017).

16. Y. Pan, *et al.*, Survival of tissue-resident memory T cells requires exogenous lipid uptake and metabolism. *Nature* **543**, 252–256 (2017).

17. J. J. Milner, *et al.*, Heterogenous Populations of Tissue-Resident CD8+ T Cells Are Generated in Response to Infection and Malignancy. *Immunity* **52**, 808-824.e7 (2020).

18. J. J. Milner, *et al.*, Runx3 programs CD8+ T cell residency in non-lymphoid tissues and tumours. *Nature* **552**, 253–257 (2017).

19. M. Andreatta, *et al.*, Interpretation of T cell states from single-cell transcriptomics data using reference atlases. *Nat Commun* **12**, 2965 (2021).